Journal of Inorganic Biochemistry 197 (2019) 110703

Contents lists available at ScienceDirect

Journal of Inorganic Biochemistry

journal homepage: www.elsevier.com/locate/jinorgbio

Design, synthesis, and evaluation of phosphorescent Ir(III) complexes with anticancer activity☆

Zhe Liu[a,*,1], JuanJuan Li[a,1], XingXing Ge[a], Shumiao Zhang[a], Zhishan Xu[a,b], Wenyuan Gao[a]

[a] Institute of Anticancer Agents Development and Theranostic Application, The Key Laboratory of Life-Organic Analysis and Key Laboratory of Pharmaceutical Intermediates and Analysis of Natural Medicine, Department of Chemistry and Chemical Engineering, Qufu Normal University, Qufu 273165, China
[b] Department of Chemistry and Chemical Engineering, Shandong Normal University, Jinan 250014, China

A B S T R A C T

A range of phosphorescent Ir(III) complexes containing four diverse PˆP-chelating ligands of the type $[Ir(ppy)_2(L)][PF_6]$, (ppy = 2-phenylpyridine) where L is 1,2-bis (diphenylphosphino)benzene (L1), 1,2-bis(diphenylphosphino)ethane (L2), 1,2-bis(diphenylphosphino)propane(L3) and 1,8-bis(diphenylphosphino)naphthalene (L4) were synthesized respectively. The iridium complexes possessed excellent antiproliferative properties, which was a substantial improvement over cisplatin, especially complex **Ir1**. Generally, the order of in vitro antiproliferative activity of the complexes is **Ir1** > **Ir2** = **Ir3** > **Ir4** > CDDP (Cisplatin). Two X-ray crystal structures were determined. The best complex, **Ir1**, was chosen to further study the mechanism of action. The self-luminescence of complex **Ir1** was also successfully used to elucidate the subcellular localization. Complex **Ir1** was specifically targeted to lysosomes in A549 cancer cells. This targeting caused lysosomal damage and the induction of ROS (reactive oxygen species) production in cancer cells. Flow cytometry studies confirmed that this complex induced apoptosis, especially late apoptosis. Our results suggested that changes in the mitochondrial membrane potential were responsible for apoptosis. The chemistry and biological studies showed that this class of metal complexes is worthy of further exploration to design novel anticancer drugs.

1. Introduction

Chemotherapy is one of the most commonly used cancer treatment methods. Cisplatin, carboplatin and oxaliplatin were approved by FDA (Food and Drug Administration), and they are called first-line chemotherapies. However, the therapeutic efficacies of these drugs are plagued by serious toxic side effects and accompanying drug resistance [1–5]. On the other hand, metal-based anticancer drugs have aroused wide research interest due to their high efficacy in treating numerous types of cancers throughout recent decades. Scientists have made tremendous efforts to search for a wide range of transition metals, such as ruthenium(II), rhodium(III), iridium(III) and ruthenium(III), which are more potent, differ from the anticancer mechanism of cisplatin and have fewer side effects [6–9]. Therefore, iridium (Ir) and ruthenium (Ru) complexes that have different mechanisms of action and cellular targets have recently had a major impact on drug development [10–16]. Cellular organelles, including the mitochondria, endoplasmic reticulum, lysosome and nucleus, are essential parts of cellular structure and normal function. [17] In light with this, metal complexes for bioapplications of organelle targeting have attracted increasing attention in recent years. Metal complexes for organelle-targeting can detect drug transport, distribution and metabolism in cells due to their superior photophysical properties, including long emission lifetimes high quantum yields and large Stokes shifts [18,19].

Over the past half-century, the metal complexes possessing NˆN, OˆN, PˆS and OˆO -chelating ligands have made considerable progress [20–27]. However, the complexes containing PˆP-chelating ligands were less studied [28]. Our previous work showed that half-sandwich complexes bearing BINAP (2,20-bis(diphenylphosphino)-1,10-binaphthyl) as PˆP-chelating ligands possess very promising anticancer properties [14]. It is necessary to develop novel metal phosphorus complexes that not only possess organelle targeting properties but also have high anticancer activities. In this work, one encouraging strategy is to integrate the introduction of PˆP-chelating ligands into the emissive iridium complexes as organelle-targeting theranostic agents. We synthesized and characterized a series of metallocompounds as anticancer agents. These complexes displayed potent antiproliferative activity and specifically target and damage lysosomes. Apart from these studies, the effects of these complexes on cancer cell toxicity, cell cycle, mitochondrial membrane potential (MMP), ROS (reactive oxygen species) and apoptosis were also investigated. The results suggest that this class of iridium complexes is useful for developing new anticancer agents.

☆ The authors declare no competing financial interest.

* Corresponding author.
E-mail address: liuzheqd@163.com (Z. Liu).

[1] The first two authors are equal first authors.

https://doi.org/10.1016/j.jinorgbio.2019.110703
Received 20 February 2019; Received in revised form 26 April 2019; Accepted 1 May 2019
Available online 04 May 2019
0162-0134/ © 2019 Elsevier Inc. All rights reserved.

2. Results and discussion

2.1. Syntheses

Four phosphorescent Ir(III) complexes containing diverse PˆP-chelating ligands of the type ($[Ir(ppy)_2(L)]PF_6$ (**Ir1–Ir4**)), where ppy is 2-phenylpyridine, L is 1,2-bis(diphenylphosphino)benzene (L1), 1,2-bis (diphenylphosphino)ethane (L2), 1,2-bis(diphenylphosphino)propane (L3) and 1,8-bis(diphenylphosphino)naphthalene (L4), were synthesized using similar methods from the literature [2]. Briefly, two equivalents of the bis-diphenylphosphine ligand and the corresponding cyclometalated Ir(III) dimer were refluxed in CH_3OH for 6 h, followed by anion exchange with NH_4PF_6, purification by recrystallization. A series of cyclometalated Ir^{III} complexes containing four diverse PˆP-chelating ligands was characterized. All the complexes were characterized using ^1H NMR (Nuclear magnetic resonance spectra), elemental analyses (C, H and P) and mass spectroscopy (MS). All the complexes were newly synthesized and isolated as PF_6^- salts. The ^1H NMR (500 MHz) spectra of complexes **Ir1–Ir4** are shown in Figs. S1–S4.

2.2. X-ray crystal structures and photophysical studies

Single crystals of **Ir1** and **Ir3**, which were suitable for X-ray diffraction analysis, were grown by slow diffusion of hexane into a saturated dichloromethane solution of the complexes. The X-ray crystal structures were determined, and their structures and atom numbering schemes are shown in Fig. 1b (CCDC 1893893, 1,893,894 contains the supplementary crystallographic data for **Ir1** and **Ir3**. These data such as selected bond lengths and angles of complexes can be obtained free of charge from The Cambridge Crystallographic Data Centre). The X-ray crystal structures of **Ir1** and **Ir3** were determined at room temperature. Consistent with an expected structure, the iridium centres in **Ir1** and **Ir3** adopt a distorted octahedral geometry where the two phosphorus atoms of the P-P ligand are trans to the carbon atoms of the C-N ligands. The two nitrogen atoms of the C-N ligands are trans to each other.

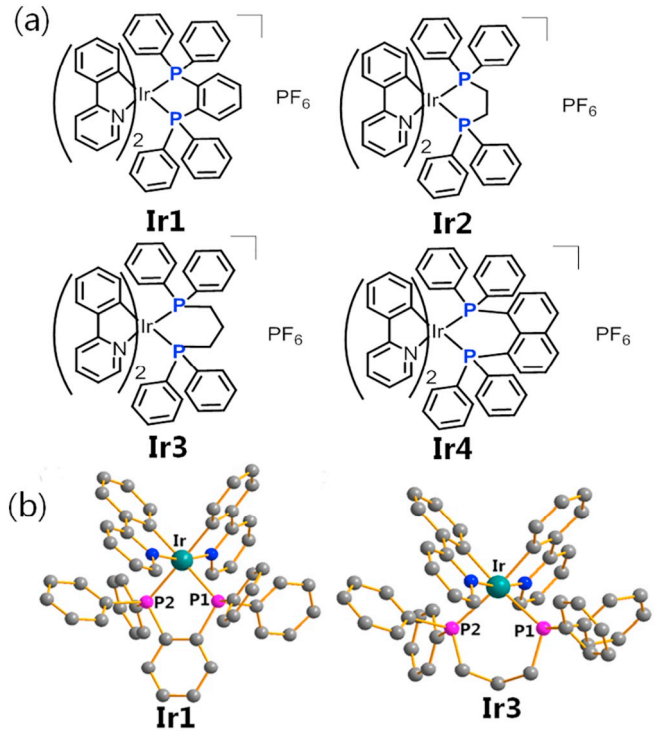

Fig. 1. (a) Chemical structures of **Ir1–Ir4**. (b) X-ray crystal structures of **Ir1** and **Ir3** set at 30% probability. The H atoms, counterions, and solvent molecules are omitted for clarity.

UV–Vis spectra and emission spectra of complexes **Ir1–Ir4** were obtained in degassed 20% MeOH/80% PBS (phosphate buffer saline) (v/v) and CH_3CN solutions at room temperature and listed in Fig. 2. As shown in Fig. 2, **Ir1–Ir4** show intense absorption bands at 250–400 nm assigned to spin-allowed intraligand transitions and spin forbidden metal-to-ligand charge transfer transitions (^{1}MLCT/^{3}MLCT) (Fig. 2). Upon excitation at 365 nm, **Ir1**, **Ir2** and **Ir4** exhibit weak luminescence with the maxima ca. 470 nm and 500 nm in 20% MeOH/80% PBS (v/v). **Ir3** display much stronger emission ca. 400 nm in 20% MeOH/80% PBS (v/v) solution compared to other metal complexes.

2.3. Cytotoxicity

The cytotoxicity of complexes **Ir1–Ir4** at various concentrations for 24 h towards A549 human lung cancer cell lines was investigated by means of MTT (3-(4,5-dimethylthiazol-2-yl)-2,5-dipheny ltetrazolium bromide) assay. To compare the toxicities, the IC_{50} (concentration where 50% of the cell growth is inhibited) values of cisplatin (CDDP) were determined on the same cell lines, and the results are listed in Table 1 and Fig. 3. It is notable that all the complexes displayed much higher potency than cisplatin against A549 cell lines, especially the complex **Ir1**. Generally, the order of in vitro antiproliferative activity of the complexes is **Ir1** > **Ir2** = **Ir3** > **Ir4** > CDDP. As shown in Table 1, it is evident that the antiproliferative activity of the complex **Ir1** containing L1 is 8.9 × higher towards A549 lung cancer cells than CDDP, showing a significant decrease in anticancer activity upon the introduction of the naphthalene group in L4. The anticancer activity of complex **Ir1** containing the PˆP-chelating ligand L1 is similar to that of the half-sandwich Ir^{III} compounds with L1 [29].

2.4. Cellular localization

The practical application of complex **Ir1** in the bioimaging of A549 cells was studied using confocal microscopy. To investigate the cellular targets of the complex, their strong green emission was used (Fig. 4). We used the Lys-specific fluorescent dye LTDR (Lyso Tracker Deep Red) or mitochondrial-specific probe MTDR (MitoTracker Deep Red) tracker for co-incubation with **Ir1** in live A549 cells. An excellent superimposition between the Lys-specific fluorescent dye LTDR and **Ir1** could be observed after incubating. The Pearson's R value of colocalization was 0.85, demonstrating that most of the complex specifically targeted lysosomes. Meanwhile, minimal colocalization of **Ir1** with the mitochondrial-probe MTDR was observed. The Pearson's R value of colocalization was 0.1. The results indicated that **Ir1** possesses lysosome targeting specificity.

2.5. Apoptosis assay

To investigate whether the antiproliferative activity observed by the MTT assay is based on apoptosis, A549 lung cancer cells were treated with complex **Ir1** at 0.5, 1, 2 and 3 equipotent concentrations of IC_{50} for 24 h, stained with annexin V/propidium iodide and analyzed using flow cytometry. This approach enabled the distinction between cells undergoing early apoptosis (stained by annexin V only, green fluorescence), viable cells (unstained, only self-fluorescence), late apoptotic cells (stained by annexin V and PI, green and red fluorescence), and nonviable cells (stained by PI (Propidium Iodide) only, red fluorescence). As shown in Fig. 5, when the complex **Ir1** at a concentration of 0.5 × IC_{50}, only 13.4% of A549 cells were in apoptotic phase in 24 h. 96.7% of A549 cells were in late apoptotic cells at 3 × IC_{50} of complex **Ir1**, whereas 93.1% was viable, indicating obvious induction of apoptosis at 3× IC_{50}.

2.6. Cell cycle analysis

Next we investigated whether the cell cycle arrest was the result of

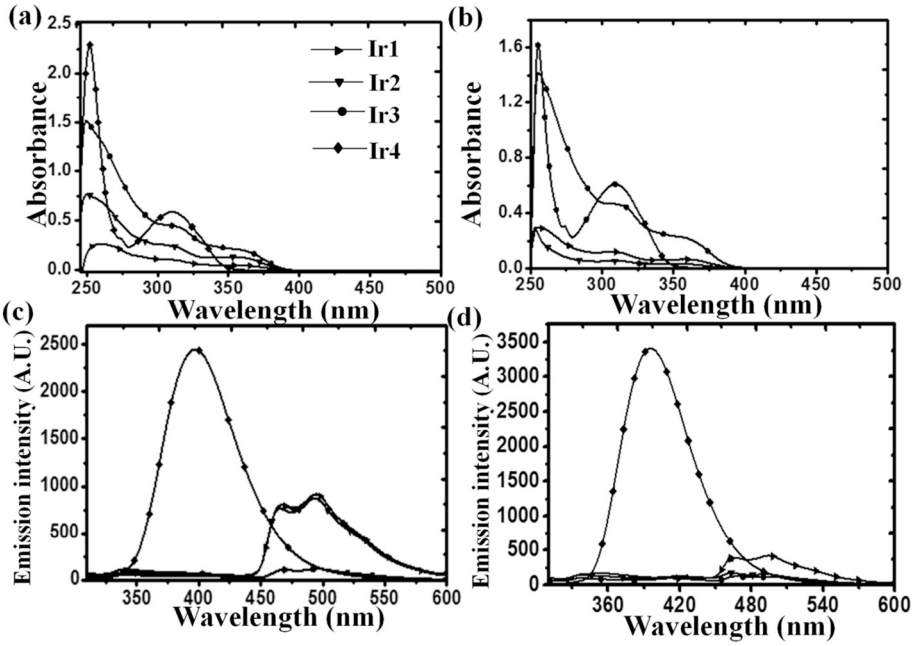

Fig. 2. UV–Vis spectrum for a 50 μM solution of complexes **Ir1–Ir4** in 20% MeOH/80% PBS (v/v) (a) and CH_3CN (b) recorded at 298 K. (c) Emission spectra for 50 μM solution of complexes **Ir1–Ir4** in 20% MeOH/80% PBS (v/v) (c) and CH_3CN (d) (λ_{ex} = 365 nm).

Table 1
Inhibition of growth of A549 cancer cells by complexes **Ir1–Ir4** and comparison with cisplatin recorded over a period of 24 h.[a]

Complex	Ir1	Ir2	Ir3	Ir4	CDDP
A549 IC_{50} (μM)	2.4 ± 0.3	2.8 ± 0.1	2.8 ± 0.6	16.5 ± 0.1	21.3 ± 1.7

[a] Cells were treated with different concentrations of the iridium complexes and cisplatin for 24 h. Cell viability was determined by the MTT assay, and data were calculated as described in the experimental section. Data are presented as means ± SD obtained in at least three independent experiments.

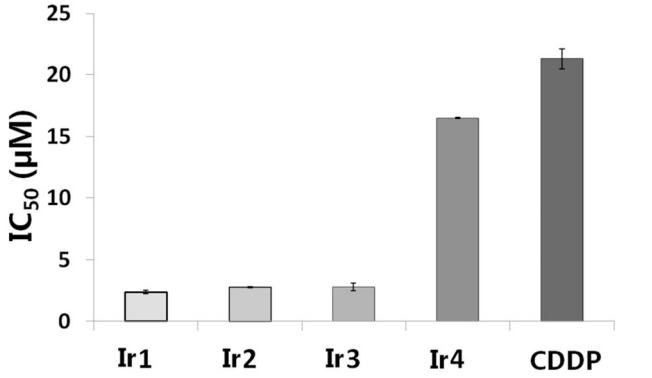

Fig. 3. Histogram showing the comparison of IC_{50} values of complexes **Ir1–Ir4** and cisplatin towards A549 cancer cells after incubation for 24 h.

inhibition of cancer cell proliferation. The cell cycle progression of A549 cancer cells after exposure with complex **Ir1** at 0.25, 0.5, 1, and 2 equipotent concentrations of IC_{50} for 24 h were analyzed by flow cytometry Fig. 6. Flow cytometric studies revealed that the percentages of cells in each cycle phase did not give discernible change, indicating that the complex **Ir1** has no effect on the cell cycle.

2.7. Mitochondrial membrane potential ($\Delta\psi_m$) changes

Lysosomal proteases were released by lysosomal damage, including cathepsin B. It has been reported that the increased release of proteases can cause the increase in mitochondrial membrane permeability and activation of the mitochondrial apoptotic pathway [30]. Therefore, we investigated the effects of complex **Ir1** on the mitochondrial membrane potential by flow cytometry analysis using the fluorescent probe JC-1. The A549 cells were co-incubated with complex **Ir1** at 0.25, 0.5, 1, and 2 equipotent concentrations of IC_{50} for 24 h. The results showed an increase in mitochondrial membrane permeability in the A549 cells in a dose-dependent manner. There were higher emission intensities of green fluorescence at 2 × IC_{50} compared to the emission intensities of control in A549 cells (Fig. 7). The experimental results showed that the complex **Ir1** induced depolarisation of the mitochondrial membrane.

2.8. Induction of intracellular reactive oxygen species (ROS)

Excessively produced ROS have been found is an important component on influence the lysosomal membrane, causing peroxidative damage to the membrane lipids, and lead to uncontrolled lysosomal permeability, along with modulation of apoptosis [31]. We further used fluorescent probe DCFH-DA (2′,7′-Dichlorodihydrofluorescein diacetate) to measure the intracellular ROS level by flow cytometry analysis. As indicated in Fig. 8, the ROS levels of A549 cells were very high even at the presence of low concentration of **Ir1** (0.25 × IC_{50}), **Ir1** exhibits excellent activity to generate ROS. These result demonstrated that **Ir1** could be used to induce oxidative damages and promote apoptosis.

3. Conclusions

In summary, the exploration of organoiridium complexes as potential anticancer drugs constitutes a rapidly growing field of research. We designed four complexes, **Ir1**-**Ir4,** and two crystal structures were reported. The study shows that all complexes exhibited potent anticancer activity towards the A549 human lung cancer cell line. Complex **Ir1** displayed the highest anticancer potency, approximately 8.9 × higher towards A549 lung cancer cells than the clinical anticancer drug cisplatin. The anticancer activity can be optimised by varying both P^P-chelated ligands. Complex **Ir1** has highly luminescent intensity, specifically targets lysosomes in A549 cancer cells and induces ROS production in cancer cells. Moreover, flow cytometry studies confirmed that the biological effects of this complex induced apoptosis,

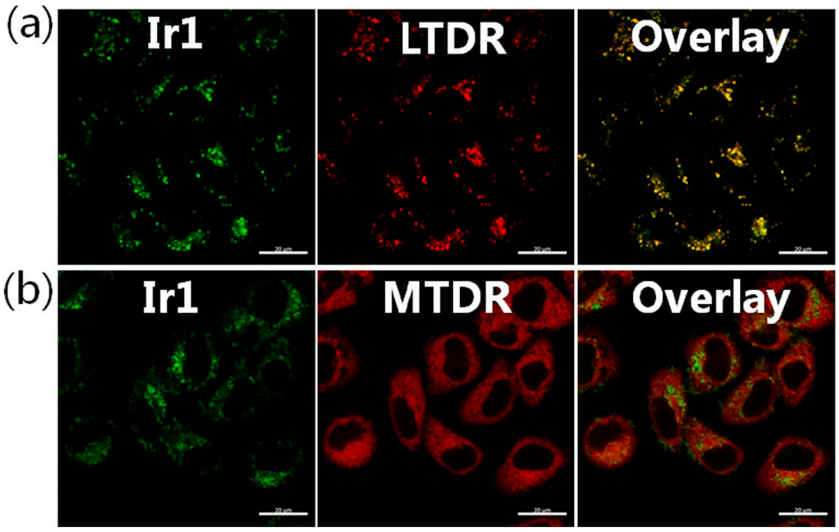

Fig. 4. (a) Confocal microscopy images of A549 cells colabeled with **Ir1**(10 μM, 0.5 h)and LTDR (100 nM, 0.5 h); (b) Confocal microscopy images of A549 cells colabeled with **Ir1**(10 μM, 0.5 h) and MTDR (75 nM, 0.5 h). The excitation and emission bands for complex: λ_{ex} = 488 nm, λ_{em} = 520 ± 30 nm; for MTDR: λ_{ex} = 644 nm, λ_{em} = 700 ± 30 nm; for LTDR: λ_{ex} = 594 nm, λ_{em} = 630 ± 30 nm. Scale bar: 20 μm.

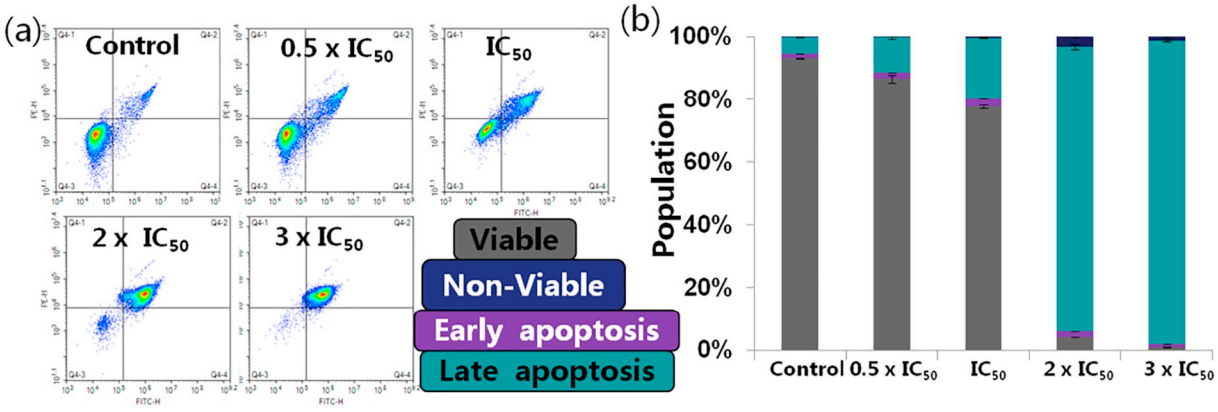

Fig. 5. Apoptosis analysis of A549 cells after 24 h of exposure to complex **Ir1** at 310 K determined by flow cytometry using annexin V vs PI staining. (A) Populations for cells treated by **Ir1**; (B) Histogram for A549 cells treated with different concentrations of metal complex **Ir1** for 24 h.

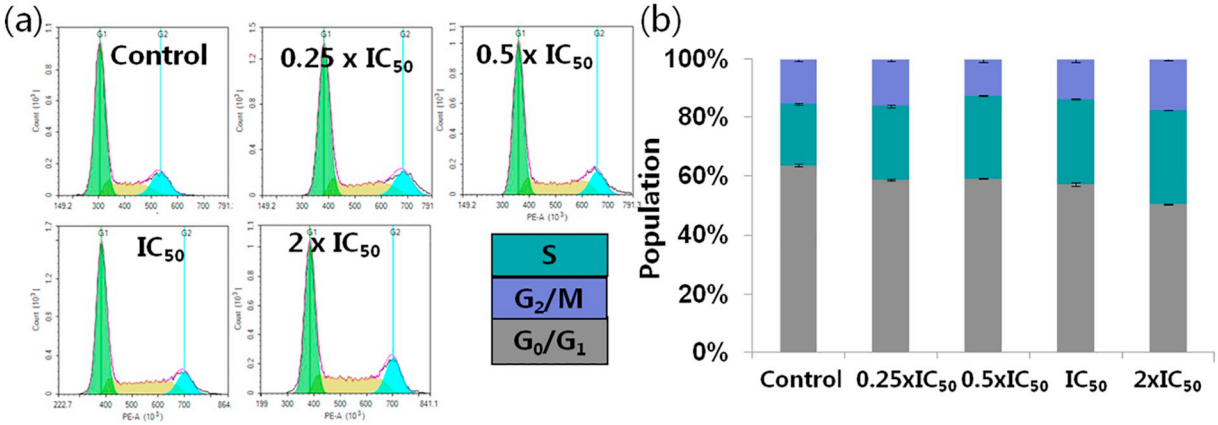

Fig. 6. Cell cycle analysis of A549 cancer cells after 24 h of exposure to complex **Ir1** at 310 K. Concentrations used were 0.25, 0.5,1 and 2 equipotent concentrations of IC_{50}. Cell staining for flow cytometry was carried out using PI. (a) FL2 histogram for control (cells untreated) and complex **Ir1** at various concentrations. (b) Cell populations in each cell cycle phase for control and complex **Ir1**.

especially late apoptosis, and that changes in the mitochondria membrane potential were responsible for apoptosis. The most detailed chemical and biological studies suggest that iridium complexes could be very effective as promising anticancer drug candidates.

4. Experimental section

4.1. Materials

Unless otherwise noted, all manipulations were performed using standard Schlenk tube techniques under nitrogen atmosphere. The reagents IrCl3•nH2O (≥99% purity), octan-1-ol (≥99%), and Nitric acid

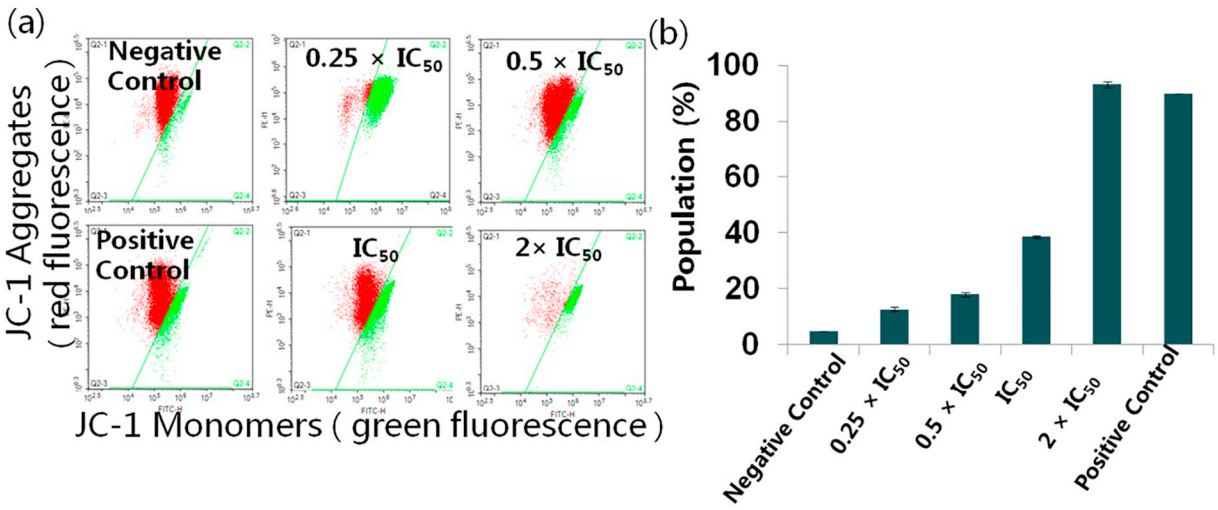

Fig. 7. Effects of complex **Ir1** on MMP analyzed by JC-1 staining and flow cytometry. A549 cells were treated with vehicle or complexes at the indicated concentrations for 24 h. The red aggregates and green monomers are gated. (a) Populations for cells treated by **Ir1**; (b) Histogram of mitochondrial membrane potential after treatment of **Ir1**. Data are quoted as mean ± SD of three replicates. (Green fluorescence indicates a decrease in MMP and red fluorescence means high membrane potentials).

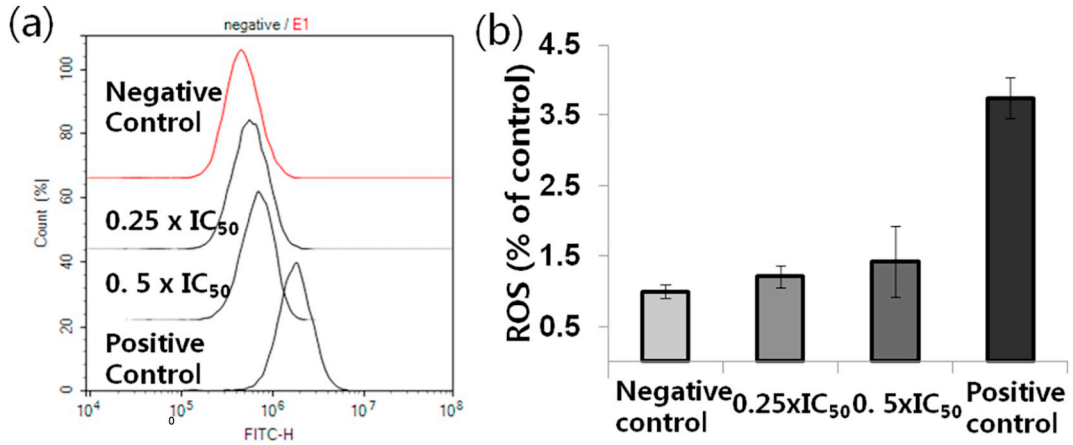

Fig. 8. Flow cytometry analysis on ROS induction in A549 cancer cells treated with complex **Ir1** at the indicated concentrations for 24 h. (a) Populations for cells treated by **Ir1**; (b) Histogram of ROS after treatment of **Ir1**. Data are quoted as mean ± SD of three replicates.

(72%), 1,2-bis(diphenylphosphino)propare (98%), 1,8-bis(diphenylphosphino)naphthalene (98%), 1,2-bis(diphenylphosphino)benzene (98%), 1,2-bis(diphenylphosphino)ethane (98%), cisplatin were purchased from Sigma-Aldrich. For the biological experiments carbonyl cyanide *m*-chlorophenylhydrazone (CCCP) were purchased from apoptosis and epigenetice company, NH_4PF_6 (Alfa Aesar), MTDR (Life Technologies), LTDR (Life Technologies), MTT (3-(4,5-dimethylthiazol-2-yl)-2,5-dipheny ltetrazolium bromide)(Sigma-Aldrich), Annexin V-FITC (fluoresceine isothiocyanate) Apoptosis Detection Kit (Sigma-Aldrich), JC-1 (Sigma-Aldrich), DCFH-DA (2′,7′-Dichlorodihydrofluorescein diacetate) (Sigma-Aldrich), PI (Propidium Iodide) (Sigma-Aldrich) were all used as received. DMEM (Dulbecco's Modified Eagle Media) medium, fetal bovine serum, penicillin/streptomycin mixture, trypsin/EDTA, and phosphate-buffered saline (PBS) were purchased from Sangon Biotech. Testing compounds was dissolved in DMSO and diluted with the tissue culture medium before use. All non-standard abbreviations are defined (Table 2).

4.2. Syntheses

The ^{1}H NMR (500 MHz) spectra of complexes **Ir1- Ir4** are shown in Figs. S1–S4.

Synthesis of the dimer: $[Ir_2(ppy)_4Cl_2]$ (ppy = 2-phenylpyridine). These compounds were synthesized using literature methods [32]. Briefly, $IrCl_3{\cdot}3H_2O$ (2.84 mmol) and ppy (6.25 mmol) were refluxed in 2-ethoxyethanol (100 mL) for 18 h. After cooling to room temperature and filtration, the residue was washed with methanol and ether. $[Ir_2(ppy)_4Cl_2]$ were obtained as yellow solids.

Synthesis of complexes **Ir1**- **Ir4**.

Ir1 ^{1}H NMR (500 MHz, DMSO-d_6) δ 8.13 (dd, J = 9.2, 6.1 Hz, 1H), 8.09 (dd, J = 5.5, 1.6 Hz, 1H), 7.84 (d, J = 8.3 Hz, 1H), 7.73–7.58 (m, 5H), 7.53 (t, J = 6.9 Hz, 2H), 7.29 (d, J = 5.8 Hz, 1H), 7.10 (t, J = 7.1 Hz, 1H), 6.99 (t, J = 7.1 Hz, 1H), 6.93 (t, J = 7.4 Hz, 1H), 6.82 (t, J = 8.9 Hz, 2H), 6.43 (t, J = 7.4 Hz, 1H), 6.27 (t, J = 8.7 Hz, 2H), 6.09 (dd, J = 7.3, 3.2 Hz, 1H). Anal. Calcd. For **Ir1** (1092.19):C, 57.19; H, 3.69; N, 2.57; found: C, 57.2; H, 3.65; N, 2.55; MS: m/z $[M\text{-}PF_6]^+$, 947.3.

Ir2 ^{1}H NMR (500 MHz, DMSO-d_6) δ 7.93 (d, J = 7.8 Hz, 2H), 7.84 (d, J = 7.9 Hz, 2H), 7.72 (dd, J = 17.8, 7.8 Hz, 6H), 7.63 (t, J = 7.8 Hz, 2H), 7.46 (t, J = 7.2 Hz, 2H), 7.35 (t, J = 7.0 Hz, 4H), 7.05 (t, J = 7.3 Hz, 4H), 6.96 (t, J = 7.4 Hz, 2H), 6.89 (t, J = 6.9 Hz, 4H), 6.63 (t, J = 8.5 Hz, 4H), 6.46 (t, J = 6.7 Hz, 2H), 6.21 (dd, J = 7.4, 3.4 Hz, 2H), 3.91 (dd, J = 29.6, 9.9 Hz, 2H), 2.91 (d, J = 10.0 Hz, 2H). Anal. Calcd. For **Ir2** (889.79): C, 49.94; H, 3.62; N, 1.57; found: C, 49.9; H, 3.65; N, 1.55; MS: m/z $[M\text{-}PF_6]^+$, 745.2.

Ir3 ^{1}H NMR (500 MHz, DMSO-d_6) δ 8.29 (d, J = 5.8 Hz, 1H), 7.75 (t, J = 8.1 Hz, 2H), 7.70–7.64 (m, 2H), 7.49 (dd, J = 18.0, 7.5 Hz, 2H),

Table 2
All non-standard abbreviations are defined.

BINAP	ppy	ROS	PBS
2,20-bis(diphenylphosphino)-1,10-binaphthyl	2-phenylpyridine	Reactive oxygen species	Phosphate buffer saline
Ir1	Ir2	Ir3	Ir4
$[Ir(ppy)_2(L1)][PF_6]$ (L1 = 1,2-bis(diphenylphosphino)benzene)	$[Ir(ppy)_2(L2)][PF_6]$ (L2 = 1,2-bis(diphenylphosphino)ethane)	$[Ir(ppy)_2(L3)][PF_6]$ (L3 = 1,2-bis(diphenylphosphino)propane)	$[Ir(ppy)_2(L4)][PF_6]$ (L4 = 1,8-bis(diphenylphosphino)naphthalene)
LTDR	MTDR	CDDP	NMR
Lyso Tracker Deep Red	MitoTracker Deep Red	Cisplatin	Nuclear magnetic resonance

7.40 (t, J = 7.2 Hz, 2H), 6.99 (t, J = 7.4 Hz, 1H), 6.86 (dt, J = 22.0, 7.1 Hz, 2H), 6.69 (dd, J = 15.2, 8.2 Hz, 3H), 6.29 (t, J = 8.1 Hz, 2H), 6.24 (d, J = 7.3 Hz, 1H), 3.27 (d, J = 7.6 Hz, 1H), 3.16–3.10 (m, 1H), 2.71 (d, J = 21.2 Hz, 1H). Anal. Calcd. For **Ir3** (1058.00): C, 55.63; H, 4.00; N, 2.65; found: C, 55.6; H, 4.05; N, 2.67; MS: m/z $[M\text{-}PF_6]^+$, 913.2.

Ir4 ^{1}H NMR (500 MHz, DMSO-d_6) δ 9.81 (d, J = 5.7 Hz, 4H), 9.54 (d, J = 5.4 Hz, 4H), 8.26 (d, J = 8.0 Hz, 4H), 8.18 (d, J = 8.1 Hz, 5H), 8.10 (t, J = 7.8 Hz, 4H), 8.01 (t, J = 7.8 Hz, 4H), 7.79 (d, J = 7.4 Hz, 6H), 7.73 (d, J = 7.5 Hz, 4H), 7.57 (t, J = 6.8 Hz, 6H), 7.45 (t, J = 6.0 Hz, 8H), 7.42–7.38 (m, 10H), 6.89 (t, J = 7.3 Hz, 4H), 6.84 (t, J = 7.4 Hz, 4H), 6.76 (t, J = 7.4 Hz, 4H), 6.69 (t, J = 7.3 Hz, 4H), 6.25 (d, J = 7.6 Hz, 4H), 5.66 (d, J = 7.5 Hz, 4H). Anal. Calcd. For **Ir3** (987.89): C, 54.71; H, 3.47; N, 1.42;found: C, 54.7; H,3.5; N, 1.45; MS: m/z $[M\text{-}PF_6]^+$, 843.2.

Acknowledgments

We thank the National Natural Science Foundation of China (Grant No. 21671118) and the Taishan Scholars Program for support.

Appendix A. Supplementary data

Supplementary data to this article can be found online at https://doi.org/10.1016/j.jinorgbio.2019.110703.

References

[1] Y. Chang, L. He, Z. Li, L. Zeng, Z. Song, P. Li, L. Chan, Y. You, X.-F. Yu, P.K. Chu, T. Chen, ACS Nano 11 (2017) 4848–4858.
[2] L. Hao, Z.-W. Li, D.-Y. Zhang, L. He, W. Liu, J. Yang, C.-P. Tan, L.-N. Ji, Z.-W. Mao, Chem. Sci. 10 (2019) 1285–1293.
[3] D. Wang, S.J. Lippard, Nat. Rev. Drug Discov. 4 (2005) 307–320.
[4] C. Licona, M.-E. Spaety, A. Capuozzo, M. Ali, R. Santamaria, O. Armant, F. Delalande, A. Van Dorsselaer, S. Cianferani, J. Spencer, M. Pfeffer, G. Mellitzer, C. Gaiddon, Oncotarget 8 (2016) 2568–2584.
[5] S. Alonso-de Castro, A.L. Cortajarena, F. López-Gallego, L. Salassa, Angew. Chem. 130 (2018) 3197–3201.
[6] B. Albada, N. Metzler-Nolte, Chem. Rev. 116 (2016) 11797–11839.
[7] J. Furrer, G. Süss-Fink, Coord. Chem. Rev. 309 (2016) 36–50.
[8] A. Bergamo, P.J. Dyson, G. Sava, Coord. Chem. Rev. 360 (2018) 17–33.
[9] V. Venkatesh, R. Berrocal-Martin, C.J. Wedge, I. Romero-Canelón, C. Sanchez-Cano, J.-I. Song, J.P.C. Coverdale, P. Zhang, G.J. Clarkson, A. Habtemariam, S.W. Magennis, R.J. Deeth, P.J. Sadler, Chem. Sci. 8 (2017) 8271–8278.
[10] Y. Huang, W. Huang, L. Chan, B. Zhou, T. Chen, Biomaterials 103 (2016) 183–196.
[11] J.-X. Liang, H.-J. Zhong, G. Yang, K. Vellaisamy, D.-L. Ma, C.-H. Leung, J. Inorg. Biochem. 177 (2017) 276–286.
[12] Y. Wang, H. Wang, H. Li, H. Sun, Application of Metallomics and Metalloproteomics for Understanding the Molecular Mechanisms of Action of Metal-Based Drugs, in: A. Mudipalli, J.T. Zelikoff (Eds.), Essential and Non-essential Metals: Carcinogenesis, Prevention and Cancer Therapeutics, Springer International Publishing, Cham, 2017, pp. 199–222.
[13] D.-L. Ma, C. Wu, W. Tang, A.-R. Gupta, F.-W. Lee, G. Li, C.-H. Leung, J. Mater. Chem. B 6 (2018) 537–544.
[14] J. Li, M. Tian, Z. Tian, S. Zhang, C. Yan, C. Shao, Z. Liu, Inorg. Chem. 57 (2018) 1705–1716.
[15] J. Li, L. Guo, Z. Tian, S. Zhang, Z. Xu, Y. Han, R. Li, Y. Li, Z. Liu, Inorg. Chem. 57 (2018) 13552–13563.
[16] J. Li, Z. Tian, X. Ge, Z. Xu, Y. Feng, Z. Liu, Eur. J. Med. Chem. 163 (2019) 830–839.
[17] K. Qiu, Y. Chen, T.W. Rees, L. Ji, H. Chao, Coord. Chem. Rev. 378 (2019) 66–86.
[18] J.-J. Cao, C.-P. Tan, M.-H. Chen, N. Wu, D.-Y. Yao, X.-G. Liu, L.-N. Ji, Z.-W. Mao, Chem. Sci. 8 (2017) 631–640.
[19] C.P. Satori, M.M. Henderson, E.A. Krautkramer, V. Kostal, M.M. Distefano, E.A. Arriaga, Chem. Rev. 113 (2013) 2733–2811.
[20] A. Habtemariam, M. Melchart, R. Fernández, S. Parsons, I.D.H. Oswald, A. Parkin, F.P.A. Fabbiani, J.E. Davidson, A. Dawson, R.E. Aird, D.I. Jodrell, P.J. Sadler, J. Med. Chem. 49 (2006) 6858–6868.
[21] Z. Tian, J. Li, S. Zhang, Z. Xu, Y. Yang, D. Kong, H. Zhang, X. Ge, J. Zhang, Z. Liu, Inorg. Chem. 57 (2018) 10498–10502.
[22] D. Kong, M. Tian, L. Guo, X. Liu, S. Zhang, Y. Song, X. Meng, S. Wu, L. Zhang, Z. Liu, J. Biol. Inorg. Chem. 23 (2018) 819–832.
[23] Y. Sun, J. Yu, X. Liu, C. Zhang, J. Cao, G. Li, X. Liu, Y. Chen, H. Huang, Biomed. Pharmacother. 102 (2018) 699–710.
[24] G. Gasser, I. Ott, N. Metzler-Nolte, J. Med. Chem. 54 (2011) 3–25.
[25] C.G. Hartinger, N. Metzler-Nolte, P.J. Dyson, Organometallics 31 (2012) 5677–5685.
[26] Q. Du, L. Guo, M. Tian, X. Ge, Y. Yang, X. Jian, Z. Xu, Z. Tian, Z. Liu,

Organometallics 37 (2018) 2880–2889.
[27] J. Li, L. Guo, Z. Tian, M. Tian, S. Zhang, K. Xu, Y. Qian, Z. Liu, Dalton Trans. 46 (2017) 15520–15534.
[28] F. Zhang, J. Jia, S. Dong, W. Wang, C.-H. Tung, Organometallics 35 (2016) 1151–1159.
[29] J. Li, Z. Tian, Z. Xu, S. Zhang, Y. Feng, L. Zhang, Z. Liu, Dalton Trans. 47 (2018) 15772–15782.
[30] R. Gómez-Sintes, M.D. Ledesma, P. Boya, Ageing Res. Rev. 32 (2016) 150–168.
[31] N. Li, L. Yu, J. Wang, X. Gao, Y. Chen, W. Pan, B. Tang, Chem. Sci. 9 (2018) 3159–3164.
[32] C. Li, M. Yu, Y. Sun, Y. Wu, C. Huang, F. Li, J. Am. Chem. Soc. 133 (2011) 11231–11239.